Physicochem. Probl. Miner. Process., 58(6), 2022, 155840

http://www.journalssystem.com/ppmp

Physicochemical Problems of Mineral Processing

ISSN 1643-1049

DE-XRT coal preparation image overlapping and adhesion particle segmentation method

Lei He, Shuang Wang , Yongcun Guo

[1] School of Mechanical Engineering, Anhui University of Science and Technology, Huainan 232001, China;

Corresponding author: shuangw094@126.com (Shuang Wang)

Abstract: Accurate segmentation of dual-energy X-ray transmission (DE-XRT) coal and gangue image regions are a prerequisite for feature extraction, identification, localization, and separation. A watershed algorithm based on multi-grayscale threshold segmentation (MGTS) is proposed to mark the foreground for the adhesion and overlap of coal and gangue. The grayscale images of foreground objects are segmented using multiple grayscale thresholds, and the number of connected domains is recorded each time. As the gray threshold value decreases, overlapping and adhering objects are gradually separated. The binary image segmented at the grayscale threshold with the most significant number of connected domains is used as a marker region. This marker region is used as the seed point of the watershed algorithm to find the dividing line. The experimental results show that the segmentation accuracy is 91.35%, and the segmentation accuracy of overlapping adhesions of 2, 3, and 4 targets is higher than 90%.

Keywords: overlap and adhesion, image segmentation, watershed algorithm; DE-XRT, coal, gangue

1. Introduction

Based on the dual-energy X-ray transmission (DE-XRT) photoelectric separation technique, the characteristic parameters of coal and gangue areas were calculated and counted for identification by image processing techniques (Yin et al., 2022). However, to calculate the image's feature parameters, it is necessary to separate the target from the graph, and the target should be a single individual (He et al., 2022). Successful separation of the target into independent individuals ensures the accuracy of feature extraction and lays the foundation for the following target localization and coal and gangue separation. In practice, many coal and gangue materials are imaged in the sorting equipment, which inevitably leads to overlap and adhesion. Therefore, how to accurately classify the overlapping and adhering targets is the first problem to be solved.

Commonly used image processing algorithms for overlapping and adhering to target segmentation include the watershed algorithm (Zhang et al., 2019) and the concave detection and matching algorithm (Sun et al., 2021). The input object of the traditional watershed algorithm is a gradient image, which will lead to serious over-segmentation because of the minimum value of the unstable region in the gradient image. Marker-based watershed algorithm is widely used to perform more reasonable segmentation of the target. The commonly used marker-based watershed algorithms include morphological watershed (Ju et al., 2022), distance transform watershed (Guo et al., 2022), and extreme erosion watershed (Abrol et al., 2021). The difference between these three algorithms is that they adopt different target foreground marking methods. Processing morphological marker foreground, using gradient images combined with open and close operations to calculate regional extremum, resulted in well foreground markers (Lin et al., 2021). For example, in the paper (Xie et al., 2019, Liang et al., 2020), the high spots (bright spots) after the morphological treatment of flotation foam were segmented into blocks. Then the seed spots were marked based on the segmented binary images of high areas. Finally, the segmentation is completed by combining the watershed algorithm. Compared with the flotation foam image, there is no bright spot in the X-ray transmission image of coal and gangue. As a result, this method is not applicable. Both distance transformation and

DOI: 10.37190/ppmp/155840

excessive corrosion are performed by operating the binary images of overlapping and adhesion targets to mark the targets. The watershed algorithm is then used to find the ridges between the targets and to complete the segmentation (Jahedsaravani et al., 2021). However, distance transformation and extreme erosion are heavily influenced by the binary image targets' shape, overlap, and adhesion level and can quickly produce false foreground markers (Liu et al., 2015). Especially for targets with irregular shapes and sizes, such as coal and gangue, the difficulty of multi-target overlap and adhesion segmentation is significantly increased. The existing concave detection methods, such as the corner detection method (Wang et al., 2015), the maximum distance method (Bai et al., 2021), the straight-line detection method (He et al., 2022), and the area threshold method (Tan et al., 2019), lose their performance advantages in the face of irregular targets such as coal and gangue. The main reason is that coal and gangue targets have depression defects of different sizes without overlap and adhesion, which affects the accuracy of depression point detection (Mebatsion et al., 2012). In addition, after the concave point detection being completed, the concave points must be matched and connected. The consumption of extended computation time will undoubtedly bring challenges to timeliness. In recent years, with the development of computer vision, some scholars have used convolutional neural networks to segment overlapping and adherent targets (Liu et al., 2021, Kubera et al., 2022). Convolutional neural networks meet the timeliness in many aspects. However, its complex network structure and many pre-trained samples still reduce the robustness of the algorithm and the ease of application in engineering.

Given this, to solve the problem of the multi-scale, multi-target overlapping and adhesion image segmentation of irregular coal and gangue, a watershed algorithm based on multi-gray threshold segmentation (MGTS) is proposed in this paper by observing the characteristics of X-ray transmission imaging of coal and gangue. The algorithm can effectively avoid the influence of the target shape and significantly improve the marking accuracy of the target. It shows good performance for overlap and adhesion segmentation problems of coal and gangue, coal and coal, and gangue and gangue with complex shapes and different thicknesses. Primarily, it can handle the problem of overlapping and adhesion segmentation of multiple targets. The essential contributions of this study are as follows:

(1) An iterative segmentation method of image marker seed points based on MGTS is proposed. It provides a new idea of seed point marking for watershed algorithms based on observing control.

(2) Combining the seed point and distance transform image, the watershed algorithm effectively segments the overlapping and adhesion targets of coal and gangue dual-energy X-rays. The accuracy rate is higher than 91%. Especially for multi-scale and multi-objective target segmentation of coal and gangue adhesion, it shows significant advantages.

(3) The limitation of iterative segmentation of image marker seed points by MGTS is analyzed, which opens up a new way for further optimization.

2. Materials and methods

2.1. Materials and experimental equipment

The coal and gangue in this paper were taken from Guqiao Coal Mine in Huainan, with particle size distribution from 5 to 500 mm and thickness distribution from 10 to 150 mm. The core components of the experimental platform for obtaining coal and gangue images include the dual-energy X-ray source of CISSY16 and the detector of CISTCQ16. The tube voltage of the X-ray source was 160kV, and the tube current was 2mA. The highest operating temperature of the emitter reached 60 ℃. The maximum power was 500W. In addition, the detector used a cadmium zinc telluride (CdZnTe) multi-level sensor with excellent photoelectric performance, which directly converted X-ray photons into electrons at room temperature. The resolution detected by the detector is 1.5 mm. There are 22 detector cards arranged underneath the X-ray source. X-rays passed first through the low-energy region of the detector card and then through the high-energy region. A copper plate was arranged between the low-energy and high-energy regions to attenuate the energy of the X-rays. Two dual-energy X-ray images were then obtained. The output image of the upper computer was a gray image with a resolution of 1000× 1088. Since only image segmentation is considered in this paper, and the low-energy region is brighter than the high-energy region, the output image of the low-energy region will be discussed as the target. Under large feeding amounts, coal and gangue particles distributed on the

belt overlap and adhesion, as shown in Fig. 1. The data used in this study were collected at a belt speed of 2.5m/s.

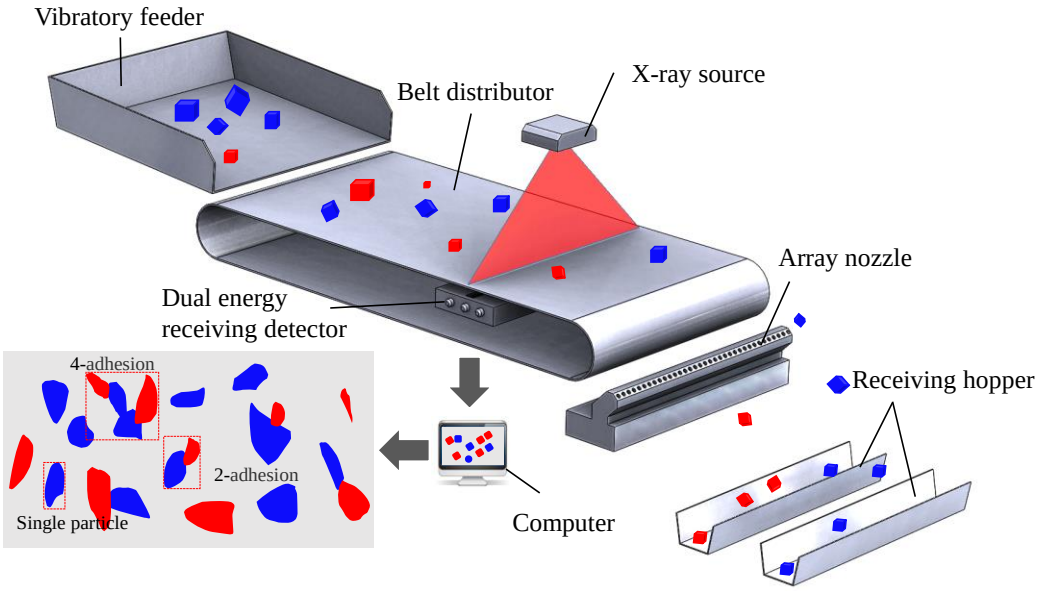

Fig. 1. Experimental image acquisition

2.2. Segmentation method of overlapping and adhesion image objects

2.2.1. XRT imaging characteristics of coal and gangue

According to the Lambert-Beer law, when X-rays penetrate a substance, it is closely related to the thickness and density of the substance (He et al., 2022). The greater the thickness and density, the weaker the radiation intensity received by the detector, which shows up in the X-ray image. The greater the thickness of coal or gangue, the smaller the grayscale pixel values. At the same thickness, the image pixels of gangue have lower grayscale values than those of coal. As shown in Fig. 2(c), the XRT imaging of coal or gangue is similar to the shape of the basin. Fig. 2(a) and (b) show the variation of the gray value of individual coal and gangue imaging pixels.

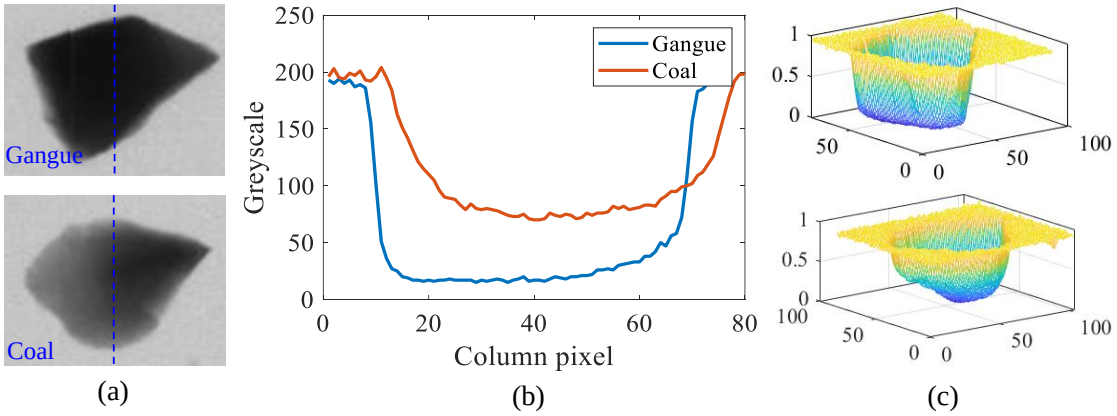

Fig. 2. Variation curve of the gray pixel value of XRT image of coal and gangue. (a) Coal and gangue; (b) Pixel variation curve in column direction; (c) Three-dimensional topographic map

As shown in Fig. 3, when the coal and gangue enter the X-ray scanning area, the pixel's gray value does not drop suddenly but slowly drops to the minimum value. There are two reasons for this: on the one hand, coal and gangue are generally spherical, thick in the middle, and thin on the sides, so the gray pixel values in the edge region are more extensive than those in the middle region. On the other hand, the caesium iodide crystals in the dual-energy X-ray detector have a delay effect when the invisible X-rays are converted to visible light, resulting in an afterglow effect (Guo et al., 2021).

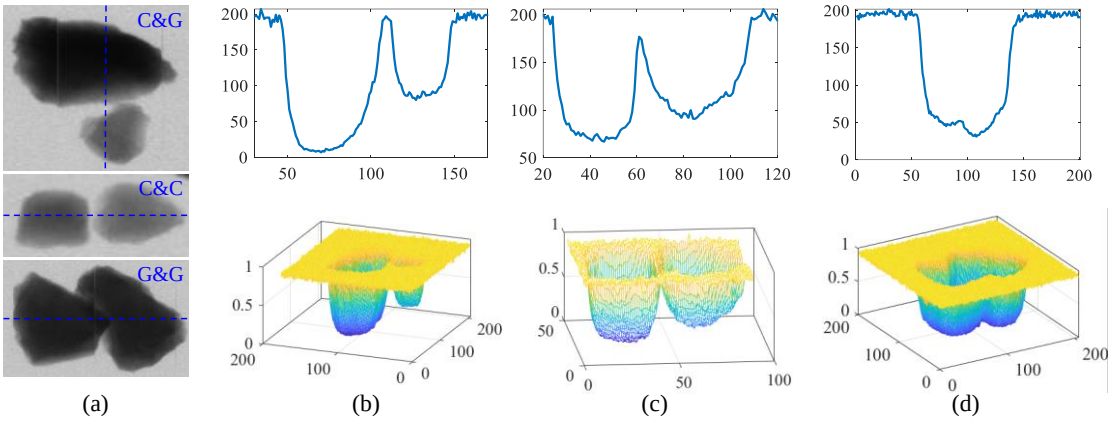

Fig. 3. Change curve of the gray value of the target pixel of coal and gangue overlap and adhesion. (a) Gray map of coal and gangue; (b), (c), (d) Row and column pixel changes and 3D topographic map

2.2.2. Watershed algorithm

The watershed algorithm is widely used in image segmentation algorithms for segmenting overlapping and adhering objects (Elsalamony et al., 2017). The idea of this algorithm can be described as follows. First, find the valley basin, i.e., the seed point (regional extremum). Then, inject water through the seed point until the water overflows into the basin. The so-called watershed is the dividing line between overlapping images and adhering images. The specific principle is shown in Fig. 4.

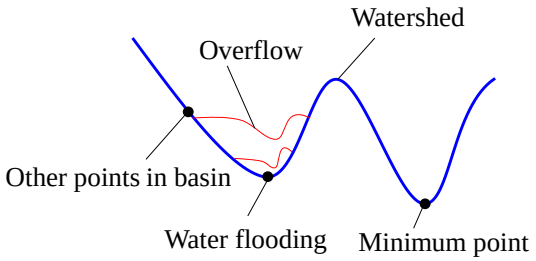

Fig. 4. Principle diagram of the watershed algorithm

2.2.3. Principle of MGTS Marking Seed Points and Watershed Segmentation

The segmentation of condensed and overlapping targets of coal and gangue images using the Watershed algorithm presupposes that the seed points, which are the extreme value regions, are found accurately. If the seed point is computed too much, it will lead to over-segmentation. If the computation is too small, it will lead to under-segmentation. This paper proposes an MGTS-based computation method that accurately marks the seed points accurately. It is described as follows.

1. The overlapped and adhered binary image is multiplied with the original grayscale image to obtain a grayscale information map without background, as shown in (a_1) and (b_1) in Fig. 6.
2. MGTS is performed on grayscale information images for connected domain detection, and the number of connected domains is recorded *con*. The set of multiple gray threshold value h and that number of record connected domains *con* is:

$$h \in \{h_1, h_2, \cdots, h_b, \cdots, h_i\} \tag{1}$$

$$con \in \{con_1, con_2, \cdots, con_b, \cdots, con_i\} \tag{2}$$

3. Selecting the gray threshold h_b with the most significant number of connected domains con_b in the MGTS process as the best threshold and taking the binary connected domain region divided by this threshold as the extreme value region, that is, the seed point. Assuming that the maximum number of connected domains is multiple, the gray value corresponding to the maximum number of connected domains for the first time is selected as the best threshold. The principle of MGTS is shown in Fig. 5.

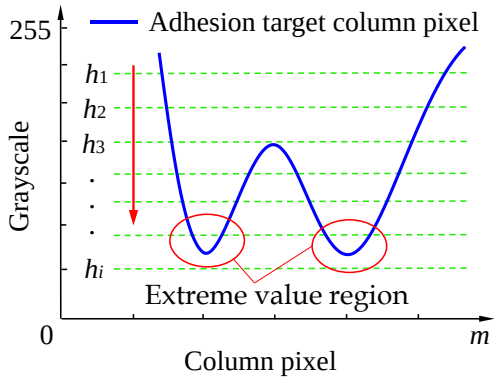

Fig. 5. Principle diagram of multiple gray threshold segmentation

Fig. 2 shows that the grayscale distribution of coal and gangue ranges from 0 to 200. The initial gray threshold h_1 is 190. Every iteration step length l is 20, and i is the number of iterations.

$$h_1 - h_i = (i-1) \cdot l \tag{3}$$

The MGTS method was used to mark the seed points. As the binary target area gradually becomes smaller, many overlapping and adhering targets begin to separate. By further lowering the threshold, smaller targets disappear. Images of the MGTS process are shown in Fig. 6. In Fig. 6, the optimal gray threshold for group (a) is h_3 = 120, and for group (b) is h_4 = 100. At this point, the segmented connected domain of the binary image is the desired seed point region.

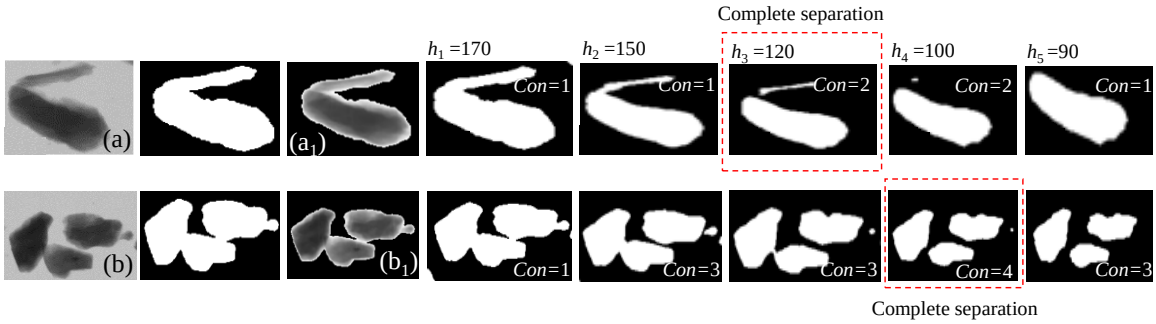

Fig. 6. Visualization of MGTS process

4. Perform a distance transformation on the overlapping adhered binary images to obtain a distance map, as shown in (b) of Fig. 7. The distance transformation process of the binary image can be described as:

The target foreground set of that binary image pixel is the record as A, the background set as B, the element value in A is 1, and the element value in B is 0. The distance transform image is D.

$$D(p) = min(disf(p,q)), p \in A, q \in B \tag{4}$$

In the equation, $disf(p, q)$ denotes the euclidean distance, and p and q are the pixel points in sets A and B. The calculation method of the euclidean distance is as follows:

$$disf(p(x_1,y_1), q(x_2,y_2)) = \sqrt{(x_1-x_2)^2 + (y_1-y_2)^2} \tag{5}$$

Using the seed point region (a) obtained in step (3) as the water injection, find the watershed ridge (c) on the distance map, and finally, complete the image segmentation. Suppose one does not choose to see the watershed on the distance map but chooses to see it on the grayscale map. In this case, the ridge will deviate. As shown in Fig. 7(e), (d) looks for ridge segmentation results on the distance map, and (e) sees ridge segmentation results on the gray map. There is a significant segmentation biasin (e).

2.2.4. Improve method for marking see points by MGTS

It is worth noting that if multiple targets adhere, the targets with small thickness will disappear after using MGTS. However, if multiple targets are still adherent, the calculation of the optimal segmenta-

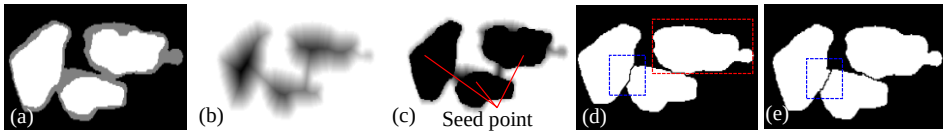

Fig. 7. Watershed algorithm segmentation. (a) Multiple gray threshold segmentation marks; (b) Distance transformation graph; (c) Water injection to find the segmentation ridge; (d) Segmentation result graph based on distance graph; (e) Segmentation result based on the gray graph

tion threshold will be wrong. If watershed segmentation is performed at this time, incorrect segmentation will occur. Alternatively, under-segmentation occurs, as shown in Fig. 7(d), because the step size l is too large. The seed point of the coal of the tiny target cannot be detected, which will also lead to under-segmentation. MGTS has difficulty getting the seed point regions of all targets with only one threshold iteration.

Therefore, after the first MGTS, a second MGTS needs to be performed: a distributed iteration is required. Assuming that the number of iterations is i, the first MGTS iteration will be performed n times. The second MGTS iteration will go from n iterations to i iterations. After the iteration to n times, the watershed algorithm is used for segmentation. At this point, the optimal grayscale threshold is h_{b1}, which corresponds to the maximum number of connected domains con_{b1}. It is determined whether the segmented connected part is a bonded or overlapping region. If it is a bonded or overlapping region, MGTS marks the seed point a second time. At this point, the optimal grayscale threshold is h_{b2}, which corresponds to *the* con_{b2} with the maximum number of connected domains. The segmentation is then performed again using the watershed algorithm.

The first iteration gray threshold set h_f.

$$h_f \in \{h_1, h_2, \cdots, h_{b1}, \cdots, h_n\} \tag{6}$$

Record the number of connected domains set con_f.

$$con_f \in \{con_1, con_2, \cdots, con_{b1}, \cdots, con_n\} \tag{7}$$

The second iteration gray threshold set h_s.

$$h_s \in \{h_n, h_{n+1}, \cdots, h_{b2}, \cdots, h_i\} \tag{8}$$

Record the number of connected domains set con_s.

$$con_s \in \{con_n, con_{n+1}, \cdots, con_{b2}, \cdots, con_i\} \tag{9}$$

2.2.5. Treatment of two special cases

When MGTS marked the seed points for the second time, there was a situation where the connected domains after MGTS could not be separated from the condensed and overlapping targets with small gray values. In this case, the number of detected connected domains is always 1, as shown in Fig. 8(i). There is also a case of insufficient segmentation, as shown in (d) in Fig. 7. In the second MGTS, the number of connected domains detected by MGTS is always 0 because of the immense value of overlapping target pixels, as shown in Fig. 8(ii). Because of the above two cases, in the second MGTS iteration, if con=0 or 1, the distance transform-based watershed algorithm will be used directly to segment the adhering and overlapping targets. Based on the distance transform image (a_1), the seed point (a_2) can be quickly calculated using the 'imextendedmin()' function in MATLAB and then segmented by the watershed algorithm.

2.2.6. Selective filtering of seed points

As shown in Fig. 9, when the gray threshold value is 100, the gray image in the figure is divided into four regions. When the threshold value is 80, it is divided into three areas. If the segmentation result when the threshold value is 100 or 80 is directly used as the marker seed point, over-segmentation will occur. This result is because the thickness of coal or gangue is not uniform, or coal is mixed with gangue. Therefore, when performing MGTS, a target will be marked as multiple seed point regions. In this paper, after finding the optimal segmentation threshold, the binary image segmented by the optimal segmentation threshold is removed by the tiny target-connected domain. According to the

area statistics of 206 seed point regions after segmentation, it is found that the number of pixels of this over-labeled seed point region is generally less than 25, accounting for 9.71%. Therefore, the area threshold for seed point filtering deletion is set to 25 in this paper.

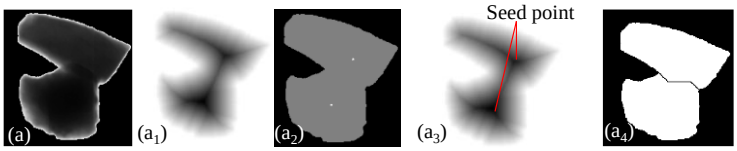

(i) Number of connected domains of the second MGTS is 1. (a) Grayscale map without background; (a_1) Distance map; (a_2) Distance transformation to calculate seed point; (a_3) Water injection to find ridge line; (a_4) Segmentation result

(ii) Number of connected domains of the second MGTS is 0. (b) Grayscale map without background; (b_1) Distance map; (b_2) Distance transformation to calculate seed point; (b_3) Water injection to find ridge line. (b_4) Segmentation result

Fig. 8. Segmentation process of distance watershed algorithm

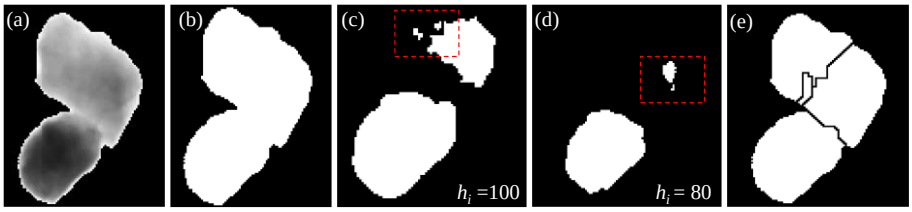

Fig. 9. Seed point selection and filtering. (a) Gray image without background; (b) Binary image; (c) Segmentation result with a threshold of 100; (d) Segmentation result with a threshold of 80; (e) Segmentation result with region marked with a threshold of 100

In summary, the flow chart of the algorithm structure of this paper is shown in Fig. 10.

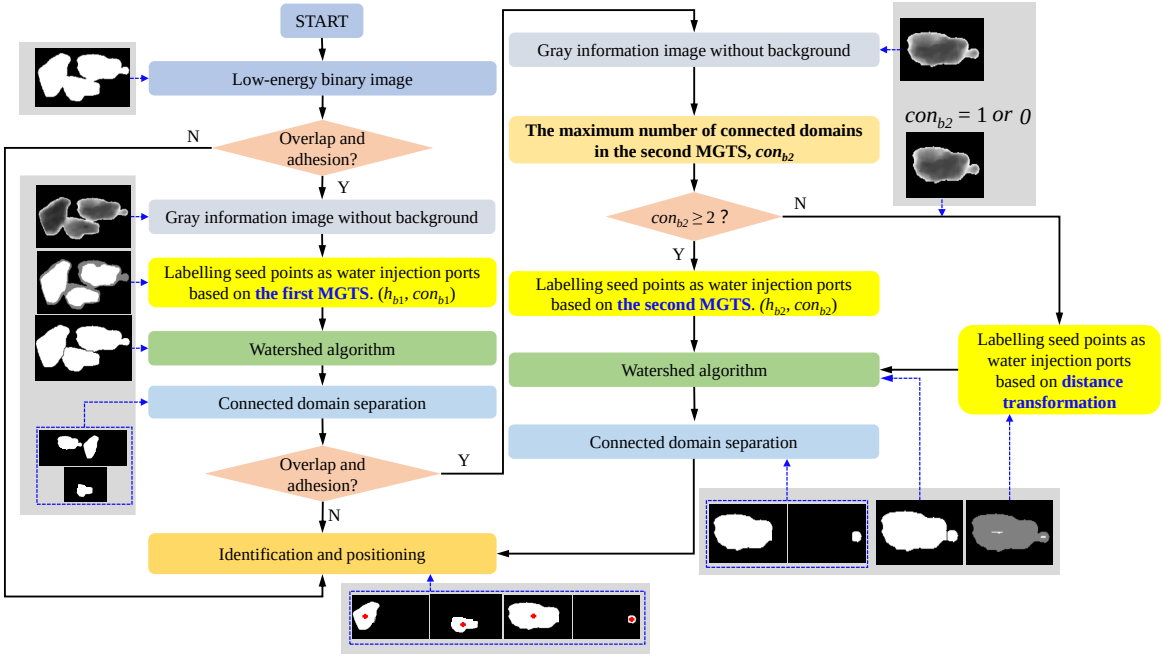

Fig. 10. Algorithm flow chart

3. Results and discussion

3.1. Segmentation results for overlapping and adhering to targets

Fig. 11 shows the segmentation results of the algorithm for overlapping and condensed objects. MGTS was performed twice, and the sequence of gray values for the first MGTS iteration was h_f= {190, 180, 170, 160, 140, 120, 100, 80, 60} with 9 iterations. The sequence of grayscale values for the second MGTS iteration is h_s = {80,60,40,20} with 4 iterations. The interval steps l between gray values are 10 and 20. In the initial iteration, the interval step l = 10 ensures that targets with a small thickness or density can be labeled smoothly. Then, step l = 20 to avoid labeling the wrong seed point region due to the small step size. The first MGTS iteration is nine times (n = 9), and the final gray threshold is 60. The setting of 60 is mainly because most coals have DE-XRT imaging gray values higher than 60 when the gray value is 60. That is to say, the first MGTS can be most of the coal and coal, coal and gangue, and other small thickness and low-density overlap adhesion target separation. In the second MGTS iteration four times, the primary purpose is to gangue, the large thickness of coal and gangue overlap, and adhesion target separation. Some of the grayscale values of the second MGTS iteration overlap with those of the first MGTS iteration. This prevents missing the seed point regions that mark low-density coal or small-thickness gangue due to small gray values during segmentation.

The initial selection of step l is large, and the marked seed points will be missed, resulting in under-segmentation. At this point, the segmentation speed is fast. Small step size selection will mark more seed points, resulting in over-segmentation. At this time, the segmentation speed is slow. Both under-segmentation and over-segmentation result in a decrease in segmentation precision, which is called error segmentation.

Choosing the number of gray thresholds n too small or too large in the first iteration can result in an erroneous selection of the optimal gray threshold. This is when some seed points are missed and under-segmentation occurs. Moreover, the choice of n has no significant influence on the algorithm speed.

In the principle of the algorithm shown in the flowchart in Fig. 10, it is necessary to determine whether there is overlap or adhesion. By default, this paper's discrimination accuracy of overlap or adhesion is 100%.

As seen in Fig. 11, the algorithm in this paper has good segmentation accuracy for overlap and adhesion segmentation of dual and multi-targets. It can solve the problems of adhesion, overlap, and

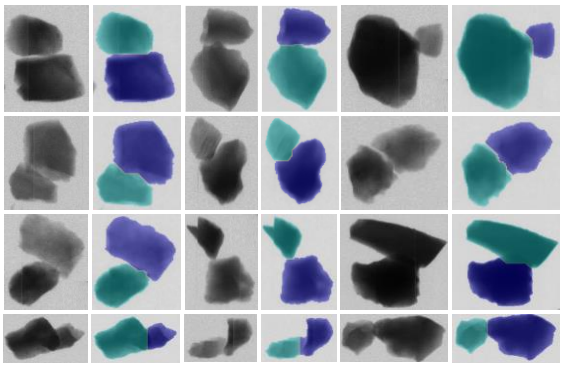

(a) 2- Target segmentation

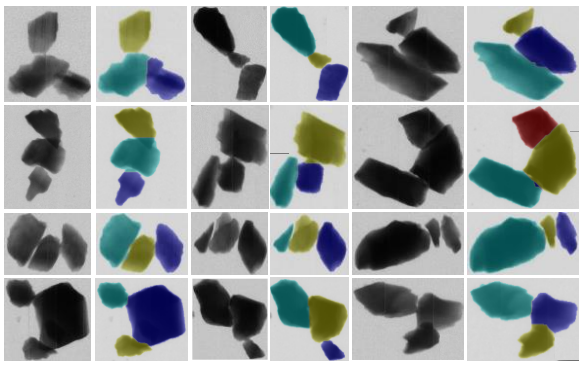

(b) 3- Target segmentation

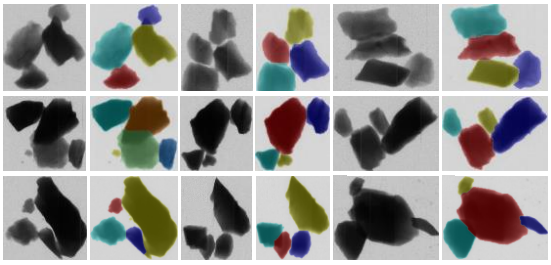

(c) 4- Target segmentation

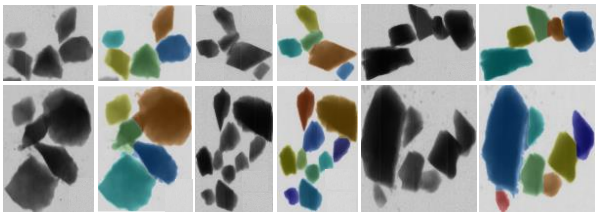

(d) +4- Target segmentation

Fig. 11. Overlapping target segmentation results

segmentation between coal and coal, coal and gangue, and gangue and gangue. It is not affected by particle size, density, and complex circumference shape.

3.2. Contrast verification

To further illustrate the algorithm's reliability for practical application, this paper compares and analyzes the segmentation accuracy of different segmentation algorithms for the same data set by setting up a comparison experiment. The data set includes 105 overlapping and adherent images of 2-objectives, 69 3-objectives, 54 4-objectives, and 15 +4-objectives for 243 images. Contrast segmentation algorithms include the watershed algorithm based on extreme erosion, the watershed algorithm based on distance transformation, and two different concave point detection and matching algorithms. Table 1 shows the segmentation results of different algorithms, and Fig. 12 compares some of the segmentation results.

Table 1. Comparison of image target results of different segmentation algorithms

Segmentation algorithm		Total	2- Target	3- Target	4- Target	+4- Target
Extreme erosion watershed algorithm	Total	243	105	69	54	15
	Error segmentation	85	21	20	34	10
	Accuracy(%)	**65.02**	**80.00**	**71.01**	**37.04**	**33.33**
Distance transform watershed algorithm	Error segmentation	54	11	11	23	9
	Accuracy(%)	**77.78**	**89.52**	**84.06**	**57.41**	**40.00**
Concave point detection and matching algorithm (Sun et al., 2021)	Error segmentation	70	18	16	23	13
	Accuracy(%)	**71.19**	**82.85**	**76.81**	**57.41**	**13.33**
Concave point detection and matching algorithm (He et al., 2022)	Error segmentation	52	11	10	19	12
	Accuracy(%)	**78.6**	**89.52**	**85.55**	**64.81**	**20.00**
The algorithm in this paper	Error segmentation	21	10	3	5	3
	Accuracy(%)	**91.35**	**90.48**	**95.65**	**90.74**	**80.00**

According to the statistics in Table 1, the algorithm in this paper can effectively segment overlapping and adhering targets, and the correct segmentation rate of 243 images reaches 91.35%. Among them, the correct rate of image segmentation for 2-target, 3-target, and 4-target is over 90%. The algorithm shows superior performance in MGTS target adhesion segmentation compared with the watershed algorithm based on extreme erosion and the watershed algorithm based on distance transformation. Compared with the distance transform watershed algorithm, the overall segmentation accuracy is improved by 13.57%. The correct segmentation of three or more overlapping and adhesion targets contributes significantly to the overall segmentation accuracy. The main reason is that MGTS iterative segmentation is used to mark the seed points, which are not affected by the complex shape of coal and gangue. Compared with the recently published method of concave point detection image segmentation (He et al., 2022), the watershed algorithm based on MGTS marked seed points has more advantages in segmentation of multi-scale, multi-target overlapping and adhesion images. For example, the segmentation accuracy of 3-target, 4-target, and more than 4-target overlapping and adhesion images has been improved by 10.1%, 25.93%, and 60%, respectively.

As seen from Fig. 12, the watershed algorithm based on extreme erosion and distance transformation to mark seed points is prone to over-segmentation or inaccurate segmentation due to the irregular shape of coal and gangue. When facing the overlap and adhesion of large and small grain size targets, it is easy to produce under-segmentation. The segmentation algorithm based on concave point detection will result in severe over-segmentation and under-segmentation due to concave point

detection and segmentation line search errors. Especially in the case of multiple targets' adhesion and large particle size differences between targets, the probability of false segmentation increases sharply.

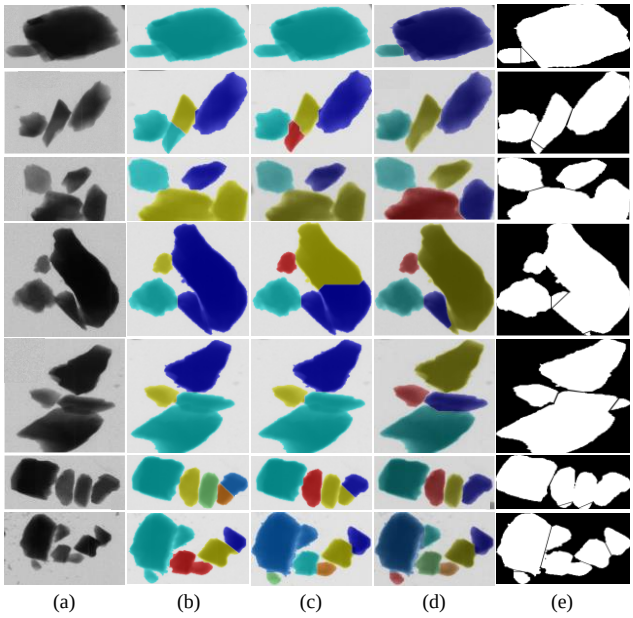

Fig. 12. Comparison of segmentation results of different segmentation algorithms. (a) Original grayscale image; (b) Watershed division of extreme corrosion; (c) Distance transform watershed segmentation; (d) The algorithm in this paper; (e) Concave point detection segmentation algorithm (He et al., 2022)

3.3. Segmentation error analysis

The key to the MGTS-based watershed algorithm proposed in this paper is the calculation and selection of seed points. Although it can significantly reduce the problems of over-segmentation and under-segmentation, there are still problems of over-segmentation for a single purpose and under-segmentation for multiple purposes.

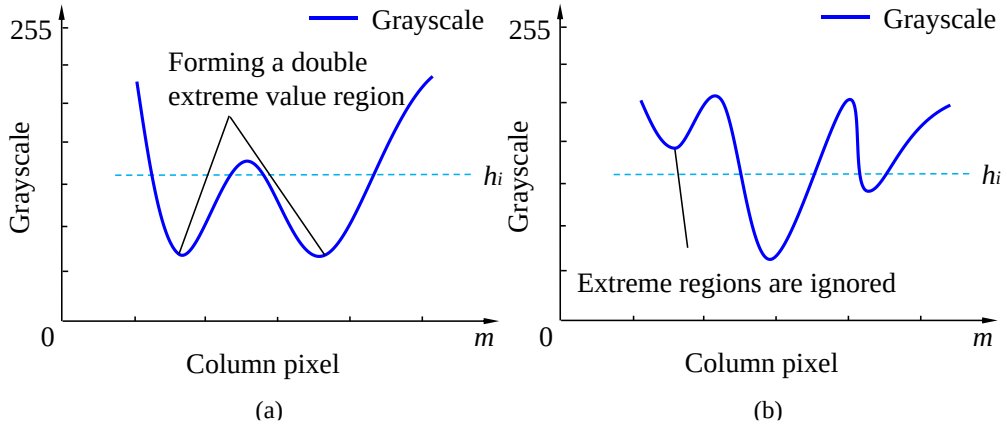

Fig. 13. Changes in pixel values. (a) The target has multiple thickness regions independently; (b) The adhesion step length *l* of the target with large and small thicknesses is larger

There are two reasons for the wrong segmentation of the target. On the one hand, a lump of single coal or gangue has multiple thicknesses. In this case, if MGTS is used, two or more extreme regions will be obtained, as shown in Fig. 13(a). In this paper, although a threshold value is set to filter out this outlier region, it is still difficult to guarantee 100% correct marking. On the other hand, when MGTS is used, the choice of step size l has an impact. If the step size is too large, in the case of multiple targets, small thicknesses of coal or gangue will be missed, resulting in insufficient segmentation, as shown in

Fig. 13(b). If the step size is too small, the inhomogeneous binary region of single coal or gangue will be divided into multiple areas, leading to over-segmentation, similar to the first reason.

As shown in Fig. 14, in (a), an extreme value region appears locally due to a considerable thickness region in one target or coal mixed with gangue, which leads to a wrong segmentation. In (b), the large-step MGTS iteration ignores it due to the slight fluctuation of the gray value of the tiny thickness target. The above errors are unavoidable, but adjusting the step size of MGTS can reduce the segmentation errors.

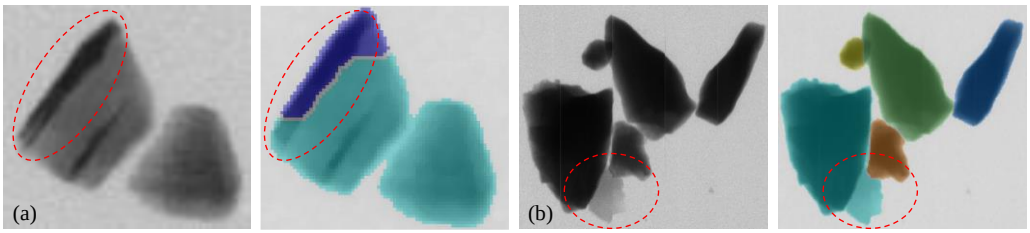

Fig. 14. Examples of wrong segmentation of objects. (a) Over-segmentation of a single object; (b) Under-segmentation of large and small thickness objects

3.4 Overview of broad application value

In this study, through observing the rules of DE-XRT image imaging of coal and gangue, a watershed algorithm based on multi-gray threshold segmentation marking seed points was designed. It solves the problem of multi-target overlap and adhesion segmentation and lays a foundation for target recognition and positioning. This method can be effectively extended to other data sets. For example, the DE-XRT technique segments other overlapped and adhesion ores (tungsten ore, copper ore, manganese ore, etc.). In addition, according to the rules of DE-XRT image imaging of coal and gangue, such a method can be extended to visible light imaging for overlap and adhesion target segmentation. For example, the flotation foam segmentation can use multiple gray threshold segmentation out bright spot areas to mark the bubble.

4. Conclusions

Based on the essential characteristics of XRT transmission imaging of coal and gangue, this paper designed a watershed algorithm based on multi-gray threshold iterative segmentation to label the foreground. It effectively solves the segmentation problem of target overlap and adhesion between coal and coal, coal and gangue, and gangue and gangue. The multi-grayscale threshold iterative segmentation to label the foreground is not affected by the shape of the target, so the labeling accuracy is high. According to the experimental statistics, gangue overlaps and adhesion segmentation accuracy is 91.35%. The segmentation accuracies of 2-target, 3-target, and 4-target are all higher than 90%, which shows the superiority in multi-target overlap and adhesion segmentation. Although there are some obvious reasons for segmentation errors, the probability of such cases is low. This problem can be solved by adjusting the step size of the multi-gray threshold or by combining it with other superior algorithms.

Acknowledgments

This work was supported by Anhui Provincial University System Innovation Project GXXT-2020-054. Lei He would like to thank his coworkers in Zhong Ke for their assistance in equipment installation and experiments.

References

YIN, J.Q., ZHU, H.Z., ZHU, J.B., ZENG, Q.Y., LI, L.S., YANG, C.G., 2022. *Analyzing the identification mechanism of graphite and clay minerale in coal and gangue using X-rays*. Physicochemical Problems of Mineral Processing, 58.

HE, L., WANG, S., GUO, Y.C, HU, K., CHENG, G., WANG, X., 2022. *Study of raw coal identification method by dual-energy X-ray and dual-view visible light imaging*. International Journal of Coal Preparation and Utilization, 1-16.

ZHANG, H., TANG, Z.H., XIE, Y.F., GAO, X.L., Chen, Q., 2019. *A watershed segmentation algorithm based on an optimal marker for bubble size measurement*. Measurement, 138182-193.

SUN, A.Y., JIA, W.B., HEI, D.Q., YANG, Y.Y., CHENG, C., LI, J.T., WANG, Z.L.,TANG, Y.J., 2021. *Application of concave point matching algorithm in segmenting overlapping coal particles in X-ray images*. Minerals Engineering, 171, 107096.

JU, A.Y., WANG, Z.L., 2022. *A novel fully convolutional network based on marker-controlled watershed segmentation algorithm for industrial soot robot target segmentation*. Evolutionary Intelligence , 1-18.

GUO, Q.P., WANG, Y.C., YANG, S.J., XIANG, Z.B., 2022. *A method of blasted rock image segmentation based on improved watershed algorithm*. scientific reports, 12 (1) , 1-21.

ABROL, V., DHALLA, S., SAINI, J., MITTAL, A., SINGH, S., GUPTA, S., 2021. *Automated segmentation of leukocytes using marker-based watershed algorithm from blood smear images*. AIJR Proceedings , 65-71.

LIN, H.B., SONG, S., TAO, S.L., LIU, H.R., 2021. *Research on Watershed Algorithm Based on Image Marking Method Optimization*. In 2021 IEEE 5th Advanced Information Technology, Electronic and Automation Control Conference (IAEAC), 5, 811-815.

XIE, D.H., LU, M., XIE, Y.F., LIU, D., LI, X., 2019. *A fast threshold segmentation method for froth image base on the pixel distribution characteristic*. PloS one, 14(1), e0210411.

LIANG, X.M., TIAN, T., LIU, W.T., NIU, F.S., 2020. *Flotation froth image segmentation based on highlight correction and parameter adaptation*. Mining, Metallurgy & Exploration, 37(2), 467-474.

JAHEDSARAVANI, A., MASSINAEI, M., MARHABAN, M.H., 2017. *An image segmentation algorithm for measurement of flotation froth bubble size distributions*. Measurement, 111, 29-37.

LIU, Z., LIU, J., XIAO, X.Y., YUAN, H., LI, X.M., CHANG, J., ZHENG, C.Y., 2015. *Segmentation of white blood cells through nucleus mark watershed operations and mean shift clustering*. sensors, 15(9), 22561-22586.

WANG, W.X., CHEN, L.Q., 2015. *Flotation Bubble Delineation Based on Harris Corner Detection and Local Gray Value Minima*. Minerals, 5 , 142-163.

BAI, F.Y., FAN, M.Q., YANG, H.L., DONG, L.P., 2021. *Image segmentation method for coal particle size distribution analysis*. Particuology, 56 , 163-170.

HE, L., WANG, S., GUO, Y.C., CHENG, G., HU, K., ZHAO, Y.Q., WANG, X., 2022. *Multi-scale coal and gangue dual-energy X-ray image concave point detection and segmentation algorithm*. Measurement, 196 , 111041.

TAN, S.Y., MA, X., MAI, Z.J., QI, L., WANG, Y.W., 2019. *Segmentation and counting algorithm for touching hybrid rice grains*. Computers and Electronics in Agriculture, 162 , 493-504.

MEBATSION, H.K., PALIWAL, J., 2012. *Machine vision based automatic separation of touching convex shaped objects*. Computers in Industry, 63 (7) , 723-730.

LIU, Y., ZHANG, Z.L., LIU, X., WANG, L., XIA, X.H., 2021. *Efficient image segmentation based on deep learning for mineral image classification*. Advanced Powder Technology, 32(10), 3885-3903.

KUBERA, E., KUBIK-KOMAR, A., KURASIŃSKI, P., PIOTROWSKA-WERYSZKO, K., SKRZYPIEC, M., 2022. *Detection and Recognition of Pollen Grains in Multilabel Microscopic Images*. Sensors, 22(7), 2690.

GUO, Y.C., HE, L., LIU, P.Z., WANG, X., 2021. *Multi-dimensional analysis and recognition method of coal and gangue dual-energy X-ray images*. Journal of China Coal Society, 46 (1), 300-309.

ELSALAMONY, H.A., 2017. *Anaemia cells detection based on shape signature using neural networks*. Measurement, 104, 50-59.